Neil R. Bastian for helpful discussions during this work.

REFERENCES

Beinert, H., Orme-Johnson, W. H., & Palmer, G. (1978) *Methods Enzymol. 54*, 111–132.
Bradford, M. (1976) *Anal. Biochem. 72*, 248–255.
Cleland, W. W. (1979) *Methods Enzymol. 63*, 103–138.
Diekert, G. B. (1988) in *The Bioinorganic Chemistry of Nickel* (Lancaster, J. R., Jr., Ed.) p 304, VCH, New York.
Diekert, G. B., & Thauer, R. K. (1978) *J. Bacteriol. 136*, 597–606.
Diekert, G. B., & Ritter, M. (1983) *FEBS Lett. 151*, 41–44.
Diekert, G. B., Graf, E. G., & Thauer, R. K. (1979) *Arch. Microbiol. 122*, 117–120.
Drake, H. L., Hu, S.-I., & Wood, H. G. (1980) *J. Biol. Chem. 255*, 7174–7180.
Gilbert, H. F., Lennox, B. J., Mossman, C. D., & Carle, W. C. (1981) *J. Biol. Chem. 256*, 7371–7377.
Kohara, T., Koyima, S., Yamamoto, T., & Yamamoto, A. (1979) *Chem. Lett.*, 1513–1516.
Laemmli, U. K. (1970) *Nature 227*, 680–685.
Miziorko, H. M., & Behnke, C. E. (1985) *Biochemistry 24*, 3174–3179.
Pezacka, E., & Wood, H. G. (1986) *J. Biol. Chem. 261*, 1609–1615.
Pezacka, E., & Wood, H. G. (1988) *J. Biol. Chem. 263*, 16000–16006.
Ragsdale, S. W., & Wood, H. G. (1985) *J. Biol. Chem. 260*, 3970–3977.
Ragsdale, S. W., Clark, J. E., Ljungdahl, L. G., Lundie, L. L., & Drake, H. L. (1983) *J. Biol. Chem. 258*, 2364–2369.
Ragsdale, S. W., Wood, H. G., Morton, T. A., Ljungdahl, L. G., & DerVartanian, D. V. (1988) in *The Bioinorganic Chemistry of Nickel* (Lancaster, J. R., Jr., Ed.) pp 322–325, VCH, New York.
Raybuck, S. A., Bastian, N. R., Orme-Johnson, W. H., & Walsh, C. T. (1988) *Biochemistry 27*, 7698–7702.
Raybuck, S. A., Bastian, N. R., Zydowsky, L. D., Kobayashi, K., Floss, H. G., Orme-Johnson, W. H., & Walsh, C. T. (1987) *J. Am. Chem. Soc. 109*, 3171–3173.
Segel, I. H. (1975) *Enzyme Kinetics*, pp 806–864, Wiley, San Francisco.
Terlesky, K. C., Nelson, M. J. K., & Ferry, J. G. (1986) *J. Bacteriol. 168*, 1053–1058.
Terlesky, K. C., Barber, M. J., Aceti, D. J., & Ferry, J. G. (1987) *J. Biol. Chem. 262*, 15392–15395.
Wood, H. G., Ragsdale, S. W., & Pezacka, E. (1986) *Biochem. Int. 12*, 421–440.
Worrall, D. M., & Tubbs, P. K. (1983) *Biochem. J. 215*, 153–157.

Calculations of Free Energy Profiles for the Staphylococcal Nuclease Catalyzed Reaction†

Johan Åqvist and Arieh Warshel*
Department of Chemistry, University of Southern California, Los Angeles, California 90089-1062
Received October 18, 1988; Revised Manuscript Received January 31, 1989

ABSTRACT: Calculations of the free energy profile for the first two (rate-limiting) steps of the staphylococcal nuclease catalyzed reaction are reported. The calculations are based on the empirical valence bond method in combination with free energy perturbation molecular dynamics simulations. The calculated activation free energy is in good agreement with experimental kinetic data, and the catalytic effect of the enzyme is reproduced without any arbitrary adjustment of parameters. The enormous reduction of the activation barrier (relative to the reference reaction in water) appears to be largely associated with the strong electrostatic effect of the Ca^{2+} ion and the two arginine residues in the active site. This favorable electrostatic environment reduces the cost of the general-base catalysis step by almost 15 kcal/mol (by stabilizing the OH^- nucleophile) and then stabilizes the developing negative charge on the 5′-phosphate group in the second step of the reaction by about 19 kcal/mol. The basic features of the originally postulated enzyme mechanism (Cotton et al., 1979) are found to be compatible with the observed activation free energy. However, the proposed modification of the mechanism (Sepersu et al., 1987), in which Arg 87 interacts only with the pentacoordinated transition state, is supported by the simulations. Further calculations on the D21E mutant also give results in good agreement with kinetic data.

Understanding the molecular origin of catalytic reactivity in enzymes is one of the most interesting challenges in theoretical molecular biology and biochemistry today. Progress in this field relies heavily on the availability of high-resolution X-ray structures of relevant enzymes as well as kinetic measurements of the catalyzed reactions, both in the protein and in solution. The recent advances in site-directed mutagenesis of proteins have opened novel possibilities of probing the contributions from single amino acids or groups of residues to the enzyme's total reduction of the activation free energy barrier [e.g., Wilkinson et al. (1984), Craik et al. (1985), Wells et al. (1986), Cronin et al. (1987), and Knowles (1987)]. However, in some cases, the total catalytic effect of the enzyme active site cannot be described simply by additive contributions

† J.Å. gratefully acknowledges support from the Swedish Natural Science Research Council. Support from the National Institute of Health (Grant GM24498) is also acknowledged.

0006-2960/89/0428-4680$01.50/0

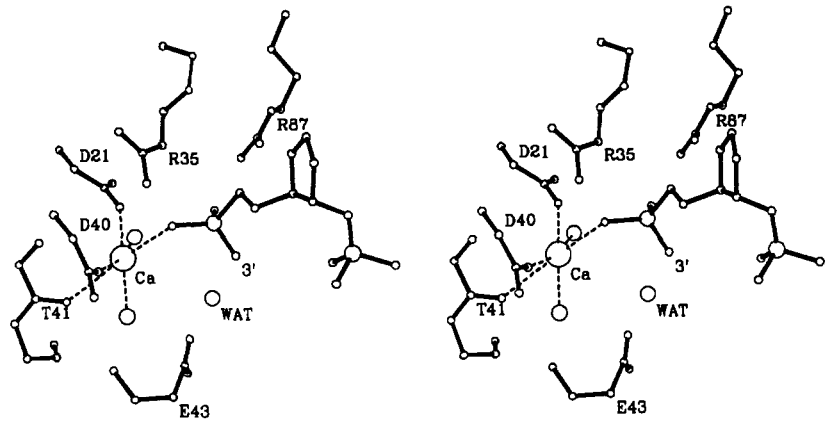

FIGURE 1: Stereoview of the active site of SNase (Cotton et al., 1979). Coordinates are from the data set 2SNS of the Brookhaven Protein Databank. The positions of the two Ca^{2+} ligated waters and the reacting water molecule have been indicated with small circles.

from individual groups, but as a coupled effect of the protein environment. From the theoretical viewpoint, the main issue is to be able to model and describe the particular enzyme system in terms of basic physical interactions in such a way that quantitative conclusions can be made concerning the reaction mechanism and the overall storage of catalytic free energies. One would like to be able to relate the reductions of free energy barriers (as compared to the reference solution reactions) to the chemical and spatial structure of the enzyme's active site. Obviously, a reliable theoretical scheme should be capable of predicting what effects mutations of different amino acids have on the rate-limiting free energy barriers.

Earlier attempts, from this laboratory, to obtain quantitative descriptions of chemical reactions in solutions and enzymes [e.g., Warshel and Levitt (1976), Warshel (1979, 1981), and Warshel and Russell (1984)] were based on implicit assumptions of linear free energy relationships [see discussion in Warshel et al. (1986)] that could not be verified by direct calculations of reaction free energies (but nevertheless now appear to be valid). Other early studies [e.g., van Duijnen et al. (1979), Kollman and Hayes (1981), and Tapia and Johannin (1981)] did not attempt to obtain quantitative results but concentrated on rigorous evaluation of isolated components of the reaction free energies. With the recent availability of supercomputers it has become possible to directly simulate chemical reactions in enzymes (Warshel, 1984a,b; Warshel & Sussman, 1986; Rao et al., 1987; Warshel et al., 1988) and solutions (Warshel, 1982; Chandrasekhar et al., 1985; Tapia & Lluch, 1985; Hwang & Warshel, 1987a; Warshel et al., 1988). In this respect, the empirical valence bond (EVB) method [e.g., Warshel and Weiss (1980) and Hwang et al. (1988)] seems particularily promising. The basic philosophy of the EVB approach is to represent the reacting system in terms of a number of simple valence bond structures that can describe the actual (ground state) potential surface on which the reaction occurs. The gas-phase parameters of these valence bond potential surfaces can be calibrated by gas-phase experiments or calculations or, when these are not available or sufficiently reliable, by use of experimental information on the relevant reactions in solution and calculated solvation energies. The effect of the surrounding (protein and/or solvent) environment on the reacting system is incorporated explicitly as a solvation term into the diagonal elements of the EVB Hamiltonian. This strategy appears to be particularily useful when applied to proteins, since it focuses on the difference between the potential surfaces in solution and in the protein. In combination with free energy perturbation molecular dynamics (FEP/MD) simulations, the EVB method provides a powerful tool which can be used to calculate free energy profiles even for reactions that involve considerable activation barriers.

In previous studies of enzyme reactions using FEP methods the main focus has been on free energy *differences* between the native and mutant enzymes along the reaction pathway (Warshel & Sussman, 1986; Rao et al., 1987; Warshel et al., 1988). It has been demonstrated that quantitative agreement with kinetic data on enzyme mutations can be achieved by this simulation approach. In this paper, we address the more general problem of calculating the absolute free energy profile, for the enzyme staphylococcal nuclease, with the EVB + FEP/MD technique.

Staphylococcal nuclease (SNase) is a single peptide chain enzyme consisting of 149 amino acid residues. It catalyzes the hydrolysis of both DNA and RNA at the 5′ position of the phosphodiester bond, yielding a free 5′-hydroxyl group and a 3′-phosphate monoester (Tucker et al., 1978):

$$H_2O + 5'\text{-}OP(O_2)^-O\text{-}3' \rightleftharpoons 5'\text{-}OH + (OH)P(O_2)^-O\text{-}3' \quad (1)$$

The enzyme requires one Ca^{2+} ion for its action and shows little or no activity when Ca^{2+} is replaced by other divalent cations (Cuatrecasas et al., 1967). A crystallographic structure at 1.5-Å resolution of SNase in complex with the inhibitor pdTp has been determined by Cotton and co-workers (Tucker et al., 1979; Cotton et al., 1979). The active site is located at the surface of the protein with the pyrimidine ring of pdTp fitting into a hydrophobic pocket while the 3′- and 5′-phosphate groups interact with several charged groups. In particular, the two arginine residues 35 and 87 donate hydrogen bonds to the 5′-phosphate, thereby partly neutralizing its double negative charge. The Ca^{2+} ion is ligated by the carboxylate groups of Asp 21 and Asp 40, the carbonyl oxygen of Thr 41, two water molecules, and one of the 5′-phosphate oxygens (Figure 1).

On the basis of this inhibited structure, a reaction mechanism for the enzyme has been postulated (Cotton et al., 1979): (I) general-base catalysis by Glu 43 which accepts a proton from a (crystallographically observed) water molecule in the second ligand sphere of the Ca^{2+} ion, yielding a free hydroxide ion; (II) nucleophilic attack by the OH^- ion on the phosphorus atom in line with the 5′-O–P ester bond leading to the formation of a trigonal-bipyramidal (i.e., pentacoordinated) transition state or metastable intermediate; (III) breakage of the 5′-O–P bond and formation of products (cf. Figure 2). This mechanism would be rate limited by the second step which in solution corresponds to an activation free energy barrier of 33 kcal/mol (Guthrie, 1977).

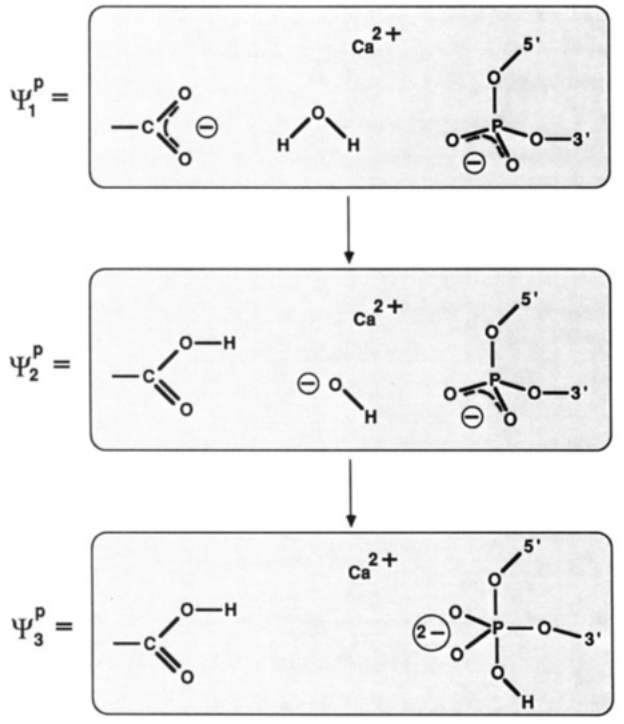

FIGURE 2: The three EVB resonance structures (Ψ_1^p, Ψ_2^p, Ψ_3^p) used to describe the catalytic reaction of SNase. The first two steps of the proposed mechanism (Cotton et al., 1979) can be described as $\Psi_1^p \rightarrow \Psi_2^p \rightarrow \Psi_3^p$.

The major difference between the inhibitor pdTp and a true substrate (in the reactant state) is the extra negative charge on the 5′-phosphate of pdTp. It therefore seems reasonable to believe that the SNase–pdTp–Ca^{2+} structure resembles the activated complex associated with the hydrolysis step rather than the reactant conformation (although it is not strictly a transition-state analogue). Sepersu et al. (1986, 1987) have examined the kinetic properties of several different SNase mutants. Their data confirm the general aspects of the proposed mechanism, indicating the importance of Glu 43 as a general-base catalyst and of the Ca^{2+} ion, Arg 35, and Arg 87 in stabilizing the transition state [it should be mentioned in this context that replacements of Glu 43 also appear to induce sizable conformational changes in the enzyme (Wilde et al., 1988)]. However, Sepersu et al. (1987) found that while both the R35G and R87G mutants reduce k_{cat} by factors of ≥35 000, only R35G affects substrate binding appreciably. They therefore suggested a slightly modified mechanism where Arg 87 interacts primarily with the trigonal-bipyramidal transition state (or metastable intermediate) and not with the 5′-phosphate group in the reactant conformation.

In spite of these minor differences, the general reaction mechanism seems clear. The overall catalytic rate constant of SNase is $k_{cat} = 95\ s^{-1}$ at $T = 297$ K corresponding to a total free energy barrier of $(\Delta g^{\ddagger}_{cat})_{obs} = 14.9$ kcal/mol. This should be compared to the pseudo-first-order rate constant for nonenzymatic hydrolysis of phosphodiester (with a water molecule as the attacking nucleophile) which is $2 \times 10^{-14}\ s^{-1}$, corresponding to $\Delta g^{\ddagger}_{(aq)} = 36$ kcal/mol (Guthrie, 1977; Kumamoto et al., 1955; Bunton et al., 1960). The rate acceleration accomplished by the enzyme is thus 10^{15}–10^{16}, which is quite impressive.

Our main objective in the present study is to calculate a reaction free energy profile for the first two (rate limiting) steps of the SNase-catalyzed reaction in the environment provided by the enzyme. We use experimental information on the relevant reference reactions in solution in order to obtain a set of EVB parameters (see below) that are constrained to reproduce the solution free energy profile. We then transfer the reacting system into the protein without any reparameterization and carry out a series of MD simulations with a mapping potential that allows us to drive the system through the different steps of the catalytic reaction. It is found that the EVB method in combination with FEP/MD simulations provides a computational scheme with which it is possible to approach quantitative agreement with the observed rate enhancement by the enzyme. The simulations also give insight into the roles of different factors contributing to the catalytic effect in SNase and elucidates the storage of the overall catalytic energy by the active site microenvironment. As an additional check of our results, the effect of the D21E Ca^{2+} ligand mutation is examined and is also found to agree well with kinetic data.

Methods

The first two steps of the SNase reaction, of which the second one is rate limiting, can be described by the three EVB resonance structures of Figure 2. Here, Ψ_1^p represents the reactant state, with Glu 43 negatively charged and the 5′-phosphate group in tetrahedral conformation. The state resulting from the general-base catalysis step, where Glu 43 has been protonated by the adjacent water molecule, is denoted by Ψ_2^p, and the pentacoordinated phosphate group formed after nucleophilic attack by the OH^- ion is denoted Ψ_3^p. The atoms depicted in the figure are considered as our solute system (S) while the rest of the protein/water environment constitutes the "solvent" (s) for the enzyme reaction. Although the Ca^{2+} ion does not actually "react", it is included in the reacting system for convenience. The diagonal elements of the EVB Hamiltonian associated with the three resonance structures (Ψ_1^p, Ψ_2^p, Ψ_3^p) can be described by the following force fields:

$$\epsilon_1 = H_{11} = \sum_i \Delta M_i^{(1)}(b_i^{(1)}) + \frac{1}{2}\sum_m K_\theta^{(1)}(\theta_m^{(1)} - \theta_0)^2 + \sum_l K_\phi^{(1)}[1 + \cos(n_l^{(1)}\phi_l^{(1)} - \delta_l^{(1)})] + V_{QQ}^{(1)} + V_{nb}^{(1)} + \alpha^{(1)} + V_{Qq,Ss}^{(1)} + V_{nb,Ss}^{(1)} + V_s$$

$$\epsilon_2 = H_{22} = \sum_i \Delta M_i^{(2)}(b_i^{(2)}) + \frac{1}{2}\sum_m K_\theta^{(2)}(\theta_m^{(2)} - \theta_0)^2 + \sum_l K_\phi^{(2)}[1 + \cos(n_l^{(2)}\phi_l^{(2)} - \delta_l^{(2)})] + V_{QQ}^{(2)} + V_{nb}^{(2)} + \alpha^{(2)} + V_{Qq,Ss}^{(2)} + V_{nb,Ss}^{(2)} + V_s$$

$$\epsilon_3 = H_{33} = \sum_i \Delta M_i^{(3)}(b_i^{(3)}) + \frac{1}{2}\sum_m K_\theta^{(3)}(\theta_m^{(3)} - \theta_0)^2 + \sum_l K_\phi^{(3)}[1 + \cos(n_l^{(3)}\phi_l^{(3)} - \delta_l^{(3)})] + V_{QQ}^{(3)} + V_{nb}^{(3)} + \alpha^{(3)} + V_{Qq,Ss}^{(3)} + V_{nb,Ss}^{(3)} + V_s \quad (2)$$

where $\Delta M_i^{(j)}$ denotes the Morse potential (relative to its minimum value) corresponding to the ith bond in the jth resonance structure. The second and third terms are the bond angle and dihedral angle bending contributions. $V_{QQ}^{(j)}$ denotes the electrostatic interaction between the solute charges and $V_{nb}^{(j)}$ the solute nonbonded interaction (other than electrostatic). The interaction energy between the solute system and the surrounding protein/water is contained in $V_{Qq,Ss}^{(j)}$ (the electrostatic part) and $V_{nb,Ss}^{(j)}$ (the rest of the nonbonded interaction). The functional forms of ΔM, V_{nb}, and V_{Qq} are given in Table I [see also Warshel et al. (1988)]. The parameter $\alpha^{(i)} - \alpha^{(j)}$ is the energy difference between Ψ_i and Ψ_j with the solute fragments at infinite separation in the gas phase. The procedure for calibration of these parameters as well as the sources of all other parameters will be discussed later in this

Table I: Parameters Used in the Calculations[a]

Morse: $\Delta M(b) = D_M[1 - e^{-\mu(b-b_0)}]^2$	
C=O (Ψ_1^p, Ψ_2^p, Ψ_3^p)	D_M = 120.0 b_0 = 1.25, μ = 2.0
C—O (Ψ_2^p, Ψ_3^p)	D_M = 83.7, b_0 = 1.36, μ = 2.0
O—H (Ψ_1^p, Ψ_2^p, Ψ_3^p)	D_M = 109.1, b_0 = 1.00, μ = 2.0
P—O (Ψ_1^p, Ψ_2^p, Ψ_3^p)	D_M = 83.7, b_0 = 1.60, μ = 2.0
P=O (Ψ_1^p, Ψ_2^p)	D_M = 120.0, b_0 = 1.49, μ = 2.0
Bond Angle: $V_\theta = (1/2)k_\theta(\theta - \theta_0)^2$	
O—P—O (Ψ_3^p)	k_θ = 100.0, θ_0 = 90°
O—P—O (Ψ_3^p)	k_θ = 100.0, θ_0 = 120°
O—P—O (Ψ_3^p)	k_θ = 100.0, θ_0 = 180°
Nonbonded: $V_{nb} = A_iA_j/r^{12} - B_iB_j/r^6$	
A_H = 0.0	B_H = 0.0
A_O = 1120.0	B_O = 24.5
A_C = 632.5	B_C = 24.5
A_P = 1500.0	B_P = 24.5
A_{Ca} = 345.0	B_{Ca} = 15.0
Nonbonded:[b] $V_{nb} = C_{ij}e^{-ar}$	
O···O (Ψ_2^p)	C_{ij} = 3600.0, a = 2.5
O···P (Ψ_2^p)	C_{ij} = 3900.0, a = 2.5
Charges: $V_{qq} = 332q_iq_j/r_{ij}$	
(O···C···O)$^-$ (Ψ_1^p)	q_O = −0.7, q_C = +0.4
H—O—C=O (Ψ_2^p, Ψ_3^p)	q_H = +0.4, q_O = −0.4, q_C = +0.4
H—O—H (Ψ_1^p)	q_H = +0.4, q_O = −0.8
(H—O)$^-$ (Ψ_2^p)	q_H = 0.0, q_O = −1.0
5′-O(HO)P(OO$^-$)O-3′ (Ψ_3^p)	q_H = 0.0, $q_{O_1} = q_{O_2} = q_{O_5}$ = −0.4, q_P = +1.0, $q_{O_3} = q_{O_4}$ = −0.9
5′-OP(OO$^-$)O-3′ (Ψ_1^p, Ψ_2^p)	$q_{O_1} = q_{O_4}$ = −0.36, q_P = +0.99, $q_{O_2} = q_{O_3}$ = −0.635
Ca^{2+} (Ψ_1^p, Ψ_2^p, Ψ_3^p)	q_{Ca} = +2.0
EVB Parameters	
H_{12}	A_{12}^{OO} = 10.0, μ_{12}^{OO} = 0.0
	A_{12}^{OH} = 0.0, μ_{12}^{OH} = 0.0
H_{23}	A_{23}^{OO} = 0.0, μ_{23}^{OO} = 0.0
	A_{23}^{OP} = 35.5, μ_{23}^{OP} = 0.0
$\alpha^{(1)}$	0.0
$\alpha^{(2)}$	21.8
$\alpha^{(3)}$	207.5

[a] Energies are in kcal/mol, distances in Å, and atomic charges in electronic charge units. Parameters not listed in the table are the same as in Warshel et al. (1988). [b] The nonbonded interaction term used for the $OH^-\cdots PO_4^-$ interaction in the EVB calculation [see Warshel and Weiss (1980)].

section. Finally, V_s represents the potential energy of the surrounding protein/solvent system.

The ground state energy E_g of the system is given by the secular equation

$$\begin{vmatrix} H_{11} - E_g & H_{12} & H_{13} \\ H_{12} & H_{22} - E_g & H_{23} \\ H_{13} & H_{23} & H_{33} - E_g \end{vmatrix} = 0 \qquad (3)$$

One of the most appealing features of the EVB method is that we can obtain values for the parameters $\alpha^{(i)}$ and the off-diagonal Hamiltonian matrix elements from experimental information on the corresponding reactions in solution. These quantities can also be determined from ab initio calculations [see discussion in Hwang et al. (1988)] or gas-phase experimental data (Warshel & Russell, 1986). However, the current reliability of ab initio calculations for medium-size reacting fragments and the limited availability of relevant gas-phase results make the direct use of solution experiments more attractive. In particular, one can notice that the gas-phase energy of the infinitely separated fragments is given by

$$\alpha^{(j)} - \alpha^{(i)} = \Delta G_{sol,w}^{(i),\infty} - \Delta G_{sol,w}^{(j),\infty} + (\Delta G_{i\to j}^{\infty})_{obs,w} \qquad (4)$$

where $\Delta G_{sol,w}^{(i),\infty}$ is the solvation free energy of the Ψ_i configuration and $\Delta G_{i\to j}^{\infty}$ is the free energy difference associated with changing Ψ_i to Ψ_j in solution, with the relevant fragments of each form kept at infinite separation. Since, in many cases, calculations of solvation free energies are more reliable than direct calculations of gas-phase energies, eq 4 can preferably be used as a starting point. A more refined implicit form of eq 4 is obtained by adjusting $\alpha^{(j)}$ until the calculated and observed values for $\Delta G_{i\to j}^{\infty}$ in solution coincide:

$$(\Delta G_{i\to j}^{\infty}(\alpha^{(j)} - \alpha^{(i)}))_{calc,w} = (\Delta G_{i\to j}^{\infty})_{obs,w} \qquad (5)$$

This procedure will be described in detail below. Once the values of the $\alpha^{(i)}$'s are calibrated with the $(\Delta G_{i\to j}^{\infty})_{obs,w}$ for the reference reaction in aqueous solution, they are kept *unchanged* when the corresponding enzymatic reaction is simulated. The actual values of the $\alpha^{(i)}$'s and other parameters in eq 2 will be considered below.

The off-diagonal matrix elements H_{ij} can also be determined by ab initio calculations [see discussion in Hwang et al. (1988)] or by semiempirical procedures [e.g., Warshel and Russell (1986)]. Here, however, we follow the simplified procedure of Hwang et al. (1988) and describe H_{ij} by a simple function:

$$H_{ij}^0 = \sum_{(k,l)} A_{ij}^{(k,l)} \exp\{-\mu_{ij}^{(k,l)} r_{kl}\} \qquad (6)$$

where the atom pair (k,l) is chosen according to the specific H_{ij}. This function is fitted to experimental information about the activation free energy for the different steps of the relevant reference reaction in solution:

$$(\Delta g_{i\to j}^{\ddagger}(H_{ij}))_{calc,w} = (\Delta g_{i\to j}^{\ddagger})_{obs,w} \qquad (7)$$

This procedure is far less reliable than that used for the diagonal energies and can benefit from ab initio calculations on the gas-phase reaction [see Hwang et al. (1988)], which can be used as extra constraints on the parameters of eq 6. However, the calculated *difference* between the free energy surface in solution and that in the enzyme is not very sensitive to the exact value of the H_{ij}'s. It has previously been demonstrated (Hwang et al., 1988) that the dependence of $\Delta g^{\ddagger}$ on the reaction free energy is almost linear. Moreover, the relation between $\Delta g^{\ddagger}$ and ΔG_0 is virtually independent of the magnitude of the particular H_{ij} [this is why linear free energy relationships were found to be so powerful in physical organic chemistry (Hammond, 1955; Albery & Kreevoy, 1978)].

A key feature of our procedure is the determination of the relevant $(\Delta G_{i\to j})_{obs,w}$ and $(\Delta g_{i\to j}^{\ddagger})_{obs,w}$ for the reference reaction in solution. In fact, quantum mechanical calculations [e.g., Warshel and Levitt (1976) and Weiner et al. (1986)] that are not calibrated by the EVB procedure would need the same free energies for verification and for reliable calibration.

The determination of the $\Delta G_{i\to j}$'s and $\Delta g_{i\to j}^{\ddagger}$'s depends, of course, on the choice of the reference reaction in solution. For instance, when one states that the rate enhancement by SNase is $\sim 10^{16}$ (Sepersu et al., 1987), one makes the implicit assumption of the reference reaction being

$$H_2O + (CH_3O)_2PO_2^- \rightleftharpoons (CH_3O)_2P(OH)_2O^- \qquad (8)$$

where the attacking species is a water molecule (from now on we only consider the reactions up to the formation of the pentacoordinated intermediate/transition state since this is the rate-limiting step). The activation free energy barrier for this reaction is 36 kcal/mol (Guthrie, 1977). This is, however, not the mechanism proposed for SNase (Cotton et al., 1979) which involves a hydroxide ion as the attacking species. A more natural choice of reference reaction in solution would therefore be

$$OH^- + (CH_3O)_2PO_2^- \rightleftharpoons (CH_3O)_2P(OH)O_2^{2-} \qquad (9)$$

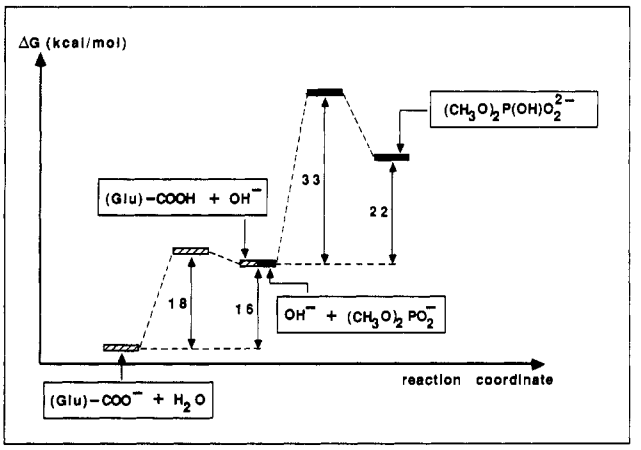

FIGURE 3: Free energy diagram based on experimental kinetic data (see text for references) for the reference solution reactions corresponding to the mechanism proposed for SNase.

This reaction requires the formation of a hydroxide ion as in the enzyme reaction. A proper reference reaction for the first step in the enzyme would then be simply the proton transfer from a water molecule to glutamic acid in solution:

$$(\mathrm{Glu})\mathrm{COO}^- + \mathrm{H_2O} \rightleftharpoons (\mathrm{Glu})\mathrm{COOH} + \mathrm{OH}^- \quad (10)$$

The reaction free energy for eq 10 is given by $(\Delta G_{1\rightarrow 2})_{\mathrm{obs,w}} = 2.3RT(\mathrm{p}K_a[\mathrm{H_2O}] - \mathrm{p}K_a[\mathrm{Glu}]) = 15.9$ kcal/mol, while the activation free energy can be estimated to be $(\Delta g^{\ddagger}_{1\rightarrow 2})_{\mathrm{obs,w}} \simeq 18.3$ kcal/mol at 297 K, with data from the reaction $\mathrm{H_2O} \rightleftharpoons \mathrm{H}^+ + \mathrm{OH}^-$ (Eigen & de Maeyer, 1955). The free energies and rate constants for formation of pentacoordinated intermediates for various phosphate ester hydrolysis reactions have been estimated and compiled by Guthrie (1977). For the hydrolysis of dimethyl phosphate by OH^- (eq 9) the obtained values are $(\Delta G_{2\rightarrow 3})_{\mathrm{obs,w}} = 22$ (±3) kcal/mol and $(\Delta g^{\ddagger}_{2\rightarrow 3})_{\mathrm{obs,w}} = 33$ kcal/mol. We thus have the reference free energy diagram depicted in Figure 3 from the experimental solution data. It should be noted that if the reaction were to proceed through exactly the same mechanism in solution as in the enzyme (including the proton transfer to a glutamic acid), the total free energy barrier would be almost 50 kcal/mol, corresponding to an enzyme rate acceleration of 10^{25}!

In order to determine the parameters $\alpha^{(l)}$ and H_{ij} that reproduce the experimentally observed free energies for the reference reactions (eq 9 and 10) in solution, we use eq 5 and 7 and the free energy perturbation method described by Warshel et al. (1988). For example, the first reaction step (eq 10) in solution can be described by the two EVB resonance structures

$$\Psi_1^{I,s} = (\mathrm{O}\cdots\mathrm{C}\cdots\mathrm{O})^- (\mathrm{H—O—H})$$

$$\Psi_2^{I,s} = (\mathrm{O{=}C—OH})\ (\mathrm{OH})^- \quad (11)$$

whose energies, ϵ_1 and ϵ_2, are given by eq 2. By introducing the mapping potential

$$\epsilon_m = \lambda_1^m\epsilon_1 + \lambda_2^m\epsilon_2 - 2|H_{12}|\sqrt{\lambda_1^m\lambda_2^m}$$

$$\lambda_1^m + \lambda_2^m = 1 \quad (12)$$

and changing the mapping vector $\vec{\lambda} = (\lambda_1,\lambda_2)$ by small increments in an MD simulation from (1,0) to (0,1), we can drive the system from the reactants via the transition state to the products. For $\vec{\lambda} = (^1/_2,^1/_2)$ the mapping potential will approach the true ground-state potential at the transition-state region, $E_g^{\ddagger} = (1/2)(\epsilon_1 + \epsilon_2) - |H_{12}|$.

The free energy associated with changing ϵ_1 to ϵ_2 can be obtained from (Zwanzig, 1954; Valleau & Torrie, 1977)

$$\delta G(\vec{\lambda}_m \rightarrow \vec{\lambda}_{m'}) = -RT \ln \langle \exp\{-(\epsilon_{m'} - \epsilon_m)/RT\}\rangle_m \quad (13)$$

$$\Delta G(\vec{\lambda}_n) = \Delta G(\vec{\lambda}_0 \rightarrow \vec{\lambda}_n) = \sum_{m=0}^{m=n-1} \delta G(\vec{\lambda}_m \rightarrow \vec{\lambda}_{m'}) \quad (14)$$

where the average $\langle\ \rangle_m$ is evaluated on the potential surface ϵ_m. Since $\Delta G(\vec{\lambda})$ represents the free energy associated with moving on the constraint potential ϵ_m, we still need to obtain the free energy, Δg, corresponding to the trajectories moving on the ground-state potential E_g. This is done with the relationship [see Warshel (1982), Hwang and Warshel (1987a), and Hwang et al. (1988)]

$$\exp\{-\Delta g(X^n)/RT\} \approx \exp\{-\Delta G(\vec{\lambda}_m)/RT\} \times \langle \exp\{-[E_g(X^n) - \epsilon_m(X^n)]/RT\}\rangle_m \quad (15)$$

where the reaction coordinate X^n can be defined in terms of the energy gap, $\Delta\epsilon = \epsilon_2 - \epsilon_1$, between the potential surfaces (Warshel, 1982; Hwang et al., 1988). This means that we calculate the energy difference between the mapping potential and the ground-state potential (given by eq 3) at each point of the MD trajectory and use the Boltzmann average of this difference to correct the free energy obtained on the mapping potential. Using $\Delta g(X^n)$, we determine the values of $(\Delta g^{\ddagger}_{1\rightarrow 2})_{\mathrm{calc,w}}$ and $(\Delta G_{1\rightarrow 2})_{\mathrm{calc,w}}$ and adjust $\alpha^{(2)}$ and H_{12}^0 until the calculated and observed values of these free energies coincide and satisfy eq 5 and 7.

For the second reaction step (eq 9) in solution we define the two EVB resonance structures as

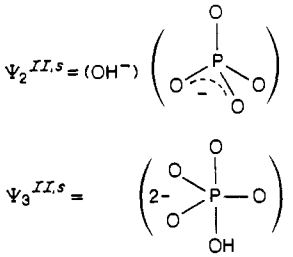

(16)

and calculate the ground-state free energy profile associated with driving the system from $\Psi_2^{II,s}$ to $\Psi_3^{II,s}$ in the same way as for the first reaction step.

Using the scheme outlined above, we thus simulate the two solution reactions (eq 9 and 10) separately, with the respective solutes immersed in a bath of 100 water molecules treated with the surface constraint all atom solvent (SCAAS) model (Warshel & King, 1985) (which is a dynamical version of earlier surface constraint models; Warshel, 1979; Warshel & Russell, 1984). The obtained values of the parameters $\alpha^{(l)}$ and H_{ij} are given in Table I together with other parameters used in the EVB calculations. The set of charges and nonbonded potential parameters in Table I were calibrated to give ion solvation free energies and nearest-neighbor distances in agreement with experimental data (e.g., see discussion of Ca^{2+} parameters at the end of this section). Those potential parameters that are not listed in Table I are taken from Warshel et al. (1988).

The next step is then to move the reacting systems into the protein environment and perform the EVB + FEP/MD calculations on the enzyme reaction steps. We now use the resonance structures (Ψ_1^p, Ψ_2^p, Ψ_3^p) of Figure 2, which represent the three relevant configurations of the proposed reaction mechanism. These resonance structures can be used to describe the entire reaction up to the formation of the pentacoordinated phosphate, since we have added the phosphate

group of $\Psi_2^{I,s}$ to $\Psi_1^{I,s}$ and $\Psi_2^{I,s}$ and the glutamic acid carboxylate group of $\Psi_2^{I,s}$ to $\Psi_2^{II,s}$ and $\Psi_3^{II,s}$. The mapping parameter vector is now $\vec{\lambda} = (\lambda_1,\lambda_2,\lambda_3)$; $\lambda_1 + \lambda_2 + \lambda_3 = 1$, where the λ_i's are the coefficients of each of the potentials ϵ_i in eq 2. In practice, only two of the λ_i's are nonzero at a given instance in the simulations. This is justified if the coupling term H_{13} is zero, as it would be in the VB formulation if terms of the second power and higher of the overlap integral S_{13} are neglected [see related case in Warshel and Weiss (1980)]. A more rigorous treatment should also consider concerted pathways, but earlier studies (Warshel & Weiss, 1980) indicate that the *difference* between the free energy of the enzyme and the solution reaction is very similar for concerted and stepwise mechanisms.

The system containing the enzyme and substrate was generated from the inhibited structure with pdTp (Cotton et al., 1979). The two Ca^{2+}-ligated waters and the reacting water molecule were initially inserted at the positions reported by Cotton et al. (1979). The protein/substrate system was partitioned into the following three regions: (I) The first is the reacting (solute) system comprising the carboxylate group of Glu 43, one water molecule, the 5′-phosphate group, and the Ca^{2+} ion (cf. Figure 2). (II) The second is a spherical region of radius ~12 Å centered on the 5′-P atom. In this region all atoms move without any restraints. All ionized residues within 9 Å from the center were treated as fully charged. The atoms in regions I and II interact with all atoms in the system, subject to a cutoff radius of 10 Å. (III) The rest of the protein atoms (not in I or II) were restrained to their crystallographic positions by harmonic potentials. The atoms in this region were only allowed to interact covalently with each other but could interact through the full nonbonded potential with atoms in I and II, provided that they were within the cutoff. Finally, a sphere of 60 (SCAAS) water molecules was created around the active site of the enzyme (the two crystallographically observed waters that ligate the Ca^{2+} ion are part of region II). The nonbonded Lennard–Jones parameters for Ca^{2+} (Table I) were obtained by performing FEP/MD calculations on the solvation of Ca^{2+} in water, requiring that they reproduce the experimentally determined solvation free energy of −381 kcal/mol (Burgess, 1978) as well as nearest-neighbor distances (Licheri et al., 1976).

The enzyme/water/substrate system was initially equilibrated for 5 ps in the product state of the second step (Ψ_3^p), since the crystallographic conformation with the doubly negatively charged pdTp is more likely to mimick the transition state than the reactants. A series of MD simulations were then carried out in which λ was changed in steps of at most 0.1 from $\vec{\lambda} = (0,0,1)$ to $\vec{\lambda} = (1,0,0)$ and in the reverse direction [$\vec{\lambda} = (1,0,0) \rightarrow \vec{\lambda} = (0,0,1)$]. At each λ point a 2-ps trajectory was calculated, of which 1 ps was used for evaluating the average in eq 15.

Results and Discussion

The calibrated free energy curve (after adjusting $\alpha^{(2)}$, $\alpha^{(3)}$, H_{12}, and H_{23}) for the two solution reactions (eq 9 and 10) obtained from the EVB + FEP/MD calculations is denoted by Δg_s and shown in Figure 4. We should again emphasize that $\Delta g_s^{\ddagger}$ does *not* correspond to the activation free energy associated with the normal hydrolysis of dimethyl phosphate (DMP) in solution but to the free energy barrier that would result if the nonenzymatic reaction proceeded through the same steps as in the enzyme. Guthrie (1977) has also estimated the rate constant for hydrolysis of DMP through the unimolecular mechanism, with an attacking water molecule as the nucleophile, to be 2×10^{-29} s^{-1} M^{-1}. Comparing this value to $\Delta g_s^{\ddagger}$

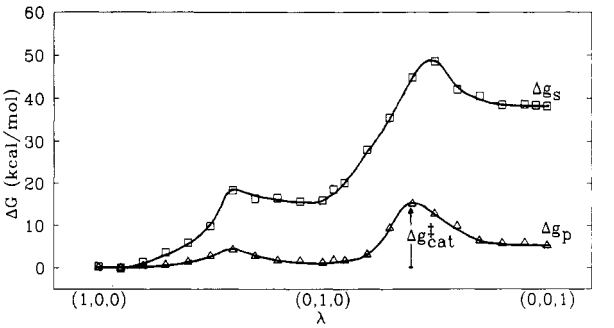

FIGURE 4: Calculated free energy profiles for the reference reaction(s) in solution (after calibration of $\alpha^{(l)}$ and H_{ij}), Δg_s, and for the enzyme reaction, Δg_p.

(Figures 3 and 4) thus reflects the difference between the general-base catalysis mechanism in solution and the case where the OH^- ion is created by abstracting a proton from a water molecule. The free energy profile Δg_p in Figure 4 is the result of transferring the reference reactions from a water cage into the protein environment. The state Ψ_1^p is described by $\vec{\lambda} = (1,0,0)$, while $\vec{\lambda} = (0,1,0)$ and $\vec{\lambda} = (0,0,1)$ denote the states Ψ_2^p and Ψ_3^p, respectively. The free energy curves in Figure 4 are calculated from the MD trajectories with eq 15 with $\vec{\lambda}$ taken as the reaction coordinate. This useful simplification is not exactly equivalent to taking $\Delta\epsilon$ as the reaction coordinate (Hwang et al., 1988). However, $\vec{\lambda}_m$ does define a particular range of the energy gap $\Delta\epsilon$, and with the use of eq 15 this choice of reaction coordinate gives the same $\Delta g^{\ddagger}$ as $\Delta\epsilon$ does, while requiring less computer time for convergence.

(*a*) *Proton Transfer Step.* The transfer of a proton from the water molecule in the second ligand sphere of the Ca^{2+} ion to its observed hydrogen-bonding partner, Glu 43, in the first step of the reaction was suggested by Cotton et al. (1979). On the basis of their previous 2-Å structure of the SNase–pdTp–Ca^{2+} complex, which involved Glu 43 as a direct ligand to the calcium, these authors (Cotton et al., 1971) had initially proposed that a hydroxide ion directly bound to the Ca^{2+} ion could serve as the nucleophile for the second step. This hypothesis was, however, not supported by any electron density (in the 2-Å map) corresponding to the proposed Ca^{2+}-bound hydroxide ion (or water molecule) adjacent to the phosphate group. Since in the refined 1.5-Å resolution map a water molecule positioned between the 5′-phosphate and Glu 43 was observed, this seemed to be a good candidate for a nucleophile, probably requiring general-base catalysis (Cotton et al., 1979). In this context one should bear in mind the fact that pdTp has an extra negative charge on the 5′-phosphate group as compared to substrates. This could make a discrimination between the two possibilities difficult because of effects of this charge on the affinity of the Ca^{2+} ion for a OH^- ligand.

The barrier of the proposed proton transfer to Glu 43 must be reduced by the enzyme by at least 3 kcal/mol, since the barrier in solution for this step is already about 18 kcal/mol (cf. Figure 3), while the *overall* barrier in the enzyme is ~15 kcal/mol. In fact, the hydroxide ion must be stabilized by much more than 3 kcal/mol (as compared to the solution reaction) in order to provide an energetically reasonable starting point for the second reaction step. Our calculated free energy profile (Figure 4) shows that the enzyme can fulfill both of these requirements. The energetic cost of the general-base catalysis step is reduced by almost 15 kcal/mol to only about 1 kcal/mol and the activation barrier by about 14 kcal/mol. This demonstrates that the proposed first step is indeed an energetically acceptable way of forming the OH^- ion. However, the major factor responsible for the free energy

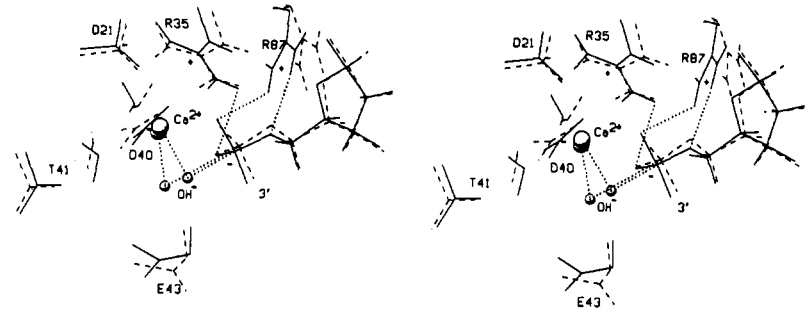

FIGURE 5: MD snapshot of the active site structure after the proton transfer step (state Ψ_2^g, dashed lines) and at the transition state of the second reaction step (full lines). The Ca^{2+} and OH^- ions are represented by dotted circles in the Ψ_2^g structure and solid circles at the transition state.

reduction in this step is the electrostatic field from the Ca^{2+} ion. The resulting OH^- ion is in our simulation stabilized by becoming directly ligated to the calcium (Figure 5). This result seems very reasonable, since the Ca^{2+} ion provides the only positive charge within such distance that it can significantly affect the proton transfer step. It seems most unlikely that the required stabilization of the OH^- ion could be achieved without its interaction with some positively charged group. Both Arg 35 and Arg 87 as well as Lys 48 appear to be too far away to exert any sizable electrostatic influence on this reaction step. The importance of the Ca^{2+} ion in stabilizing the OH^- ion, indicated by the present calculations, is also consistent with the observation that at lower Ca^{2+} concentrations the pH optimum of the catalytic reaction is shifted toward higher pH values (Cuatrecasas et al., 1967).

It is interesting to note that smaller divalent cations are much less effective in activating the enzyme (Cuatrecasas et al., 1967; Sepersu et al., 1987). For Mn^{2+}, the activation efficiency has been found to be at least a factor of 35 000 less than that of Ca^{2+} (Sepersu et al., 1987). On the other hand, the slightly larger Sr^{2+} appears to be the only ion besides calcium capable of any significant enzyme activation [Sr^{2+} can serve as an activator for DNA, but not RNA, hydrolysis (Cuatrecasas et al., 1967)]. These data could in fact reflect a direct interaction between the metal ion and the hydroxide ion resulting from the proton transfer step. A Mn^{2+} ion would bind the OH^- ion more tightly than Ca^{2+} and can therefore be assumed to lower the free energy of state Ψ_2^g more than that of the transition state of the subsequent reaction step. If the lowering of Ψ_2^g with respect to Ψ_1^g and the transition state is large enough, the Mn^{2+}-bound enzyme would be effectively inhibited as observed experimentally (Sepersu et al., 1987). Assuming that the main effect of the metal ion is on the state Ψ_2^g, the substitution of Ca^{2+} for a slightly larger ion such as Sr^{2+} (that binds the OH^- less strongly) would not be expected to affect Δg^*_{cat} as much as a smaller ion. A more serious consideration of these issues will, however, require further calculations in which Ca^{2+} is substituted for other ions.

(*b*) *Formation of the Pentacoordinated Transition State.* It is clear that SNase must provide an extremely efficient catalytic environment in order to reduce the activation barrier of the nucleophilic attack by the OH^- ion on the 5′-phosphate group. The observed barrier for the solution reaction (eq 5), $(\Delta g^*_{2\rightarrow 3})_{obs,w}$ = 33 kcal/mol (Guthrie, 1977), is 11 kcal/mol higher than that for a nucleophilic attack by OH^- on a neutral phosphate (Guthrie, 1977). This difference is most likely due to the increased electrostatic repulsion between the OH^- ion and negatively charged phosphate oxygens. The crystallographic structure of the enzyme–inhibitor complex (Cotton et al., 1979) provides a plausible explanation for how the enzyme reduces this electrostatic repulsion and catalyzes the reaction. The two arginine residues Arg 35 and Arg 87 interact closely with the doubly negatively charged 5′-phosphate of pdTp, and one of the phosphate oxygens is also ligated to the calcium ion. These positive charges should be able to, at least partially, neutralize the double negative charge associated with the formation of the transition state in the hydrolysis step.

Our calculated reaction free energy profile (Figure 4) shows a reduction of the free energy barrier associated with the second step of 19 kcal/mol, which is indeed impressive. It is also encouraging to note that the total free energy barrier (for both reaction steps) resulting from the EVB calculations, Δg^*_{cat} = 15.1 kcal/mol, is well in accord with the experimentally observed overall rate of the enzyme $(\Delta g^*_{cat})_{obs}$ = 14.9 kcal/mol. It should, however, be pointed out that this good agreement is somewhat fortuitous as our error range for the absolute value of Δg^*_p is about 5 kcal/mol. This error range is mainly determined by the errors in the experimentally evaluated reaction free energies (Guthrie, 1977) and by the convergence errors in the FEP/MD calculations.

Figure 5 shows an MD snapshot of the active site structure at $\vec{\lambda}$ = (0,1,0) (Ψ_2^g) and at $\vec{\lambda}$ = (0,0.6,0.4) (the transition state for the second step). The simulations clearly support the suggestion by Sepersu et al. (1987) that Arg 87 primarily interacts with the 5′-phosphate group in the transition state rather that with the reactant state. As can be seen from Figure 5, Arg 87 does not interact as closely with the 5′-phosphate group on the Ψ_2^g state as in the transition state, where it donates two strong hydrogen bonds to the O5′ atom and one of the free phosphate oxygens. The second arginine residue in the active site (Arg 35), however, is hydrogen bonded to the 5′-phosphate group in both the reactant (Ψ_2^g) and transition states, the interaction being somewhat strengthened at the transition state. This is consistent with the finding (Sepersu et al., 1987) that Arg 35 affects substrate binding substantially more than Arg 87 does. The calculations therefore support the idea that the SNase–pdTp–Ca^{2+} ternary complex ressembles the activated complex of the reaction (although it is not a transition-state analogue), rather than reactant conformation with a bound substrate.

It appears that the excellent "solvation" of the transition state by SNase can be described almost completely as an electrostatic effect. The loss of interaction energy between the Ca^{2+} ion and the hydroxide ion in moving toward the pentacoordinated structure is compensated for mainly by increased interaction between the Ca^{2+} ion and the 5′-phosphate oxygen ligand. The accumulating negative charge ($-1 \rightarrow -2$) on the phosphate group is effectively neutralized by closer interactions with Arg 35 and Arg 87. In particular, Arg 87 appears to be an important factor, as it hydrogen bonds strongly with two of the phosphate oxygens in the transition state while not in the reactant state. This is also evidenced

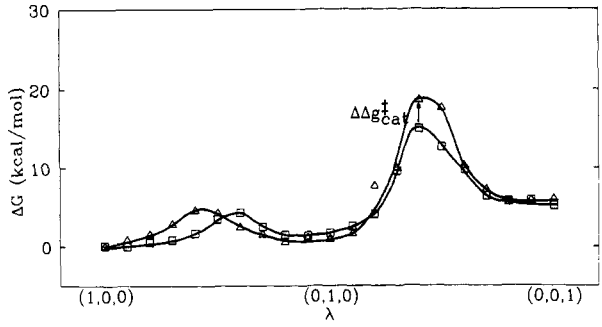

FIGURE 6: Comparison of reaction free energy profiles for the native enzyme (open squares) and the D21E mutant enzyme (open triangles).

by preliminary results from simulations of the R87G mutant (to be published elsewhere) which indicate a large effect on k_{cat} for this species.

It seems to us a bit hazardous to assign a specific catalytic contribution from each of the factors involved in the SNase reaction (Sepersu et al., 1987), since they are not totally separable from each other. Also, when interpreting kinetic experiments on mutant enzymes in the absence of accompanying structural data, it is very difficult to assess the nature of conformational changes caused by the mutations. In the case of SNase, Wilde et al. (1988) have demonstrated by NMR measurements that mutations of Glu 43 can cause conformational changes extending over considerable distances. It is therefore not evident that the contribution to the catalytic effect ascribed by Sepersu et al. (1987) to Glu 43 ($\sim 10^4$) is solely due to general-base catalysis. Judging from our calculations, it seems, however, reasonable to suggest that the Ca^{2+} ion is the most important factor (besides Glu 43) in the first step of the reaction, while both the Ca^{2+} ion and the two active site arginine residues (in particular Arg 87) play an important role in reducing the barrier of the second step. It should also be noted that the effect of Glu 43 as a general base is included in our reference reaction in the solvent cage. This type of definition therefore considers the general base as a part of the reacting system rather than as a catalytic factor. In fact, the intrinsic catalytic effect of Glu 43 as a general base *in solution* is only 5–6 kcal/mol (relative to having a water molecule as the proton acceptor) while the Ca^{2+} ion contributes with ~15 kcal/mol.

(*c*) *Calculations on the D21E Mutant.* In order to further gauge the reliability of our calculated reaction free energy profile for the native enzyme, it is interesting to examine the effects of single-site mutations. If the apparent success of our modeling study of the SNase catalytic reaction is not coincidental, the effects of amino acid substitutions on the reaction profile should be consistent with experimental kinetic data. In chosing a suitable mutant as our first test case, we have sought a mutation that does not seem to cause large structural changes in the protein, while still having an appreciable effect on k_{cat}. Sepersu et al. (1987) have characterized a number of different SNase mutants of which the D21E (Asp 21 → Glu 21) substitution appears to satisfy the above criterion. This mutation has virtually no effect on either calcium or substrate binding while reducing V_{max} to 6.7×10^{-4} of the velocity of the native enzyme. This number corresponds to an increase of the overall activation barrier by $(\Delta\Delta g^{\ddagger}_{cat})_{obs}$ = 4.3 kcal/mol.

The effect of mutations on the enzymatic activation free energy can be calculated with FEP/MD simulations using different thermodynamic cycles (Hwang & Warshel, 1987b; Rao et al., 1987; Warshel et al., 1988). One option is to slowly transform, in our case, Asp 21 into a glutamic acid at the transition state and the reactant state of the native enzyme. The difference in the free energy associated with this (nonphysical) transformation [see Warshel (1981) for early treatments using this type of cycle] will thus give the change in the catalytic free energy between the native and mutant enzymes [e.g., Hwang and Warshel (1987b), Rao et al. (1987), and Warshel et al. (1988)]. This would in our case require Asp → Glu transformations at points corresponding to both $\vec{\lambda}$ = (1,0,0) and $\vec{\lambda}$ = (0,1,0), since these states are of similar energy, as well as at the transition state $\vec{\lambda}$ = (0,0.6,0.4). However, such an approach ignores the possibility that the location of the transition state is affected by the mutation [see discussion in Warshel et al. (1988)]. We have therefore taken the more rigorous route which amounts to calculating the entire profile for the D21E mutation in the same manner as for the native enzyme. The starting conformation was taken from the pdTp-inhibited structure of SNase, in which Asp 21 was substituted for a glutamic acid by use of model building followed by extensive energy minimization.

A comparison between the calculated reaction free energy profiles for native SNase and the D21E mutant is shown in Figure 6. It can be seen that the largest effect of the substitution occurs on the second reaction step. The calculated barrier (with respect to Ψ^g_2) for the formation of the pentacoordinated phosphate is 4.4 kcal/mol higher for D21E than for the native enzyme. For the proton transfer step, the change in the free energy of the barrier and of the Ψ^g_2 state is very small ($\Delta\Delta G_{Asp\rightarrow Glu}[\vec{\lambda}=(0,1,0)]$ = −0.6 kcal/mol). This gives a total change in the overall catalytic barrier of $\Delta\Delta g^{\ddagger}_{cat}$ = +3.8 (±0.9) kcal/mol, which is well in accord with the kinetic data for the D21E mutant (Sepersu et al., 1987). The simulations indicate that an important structural effect of the enlargement of Asp 21 is a displacement of the Ca^{2+} ion of about 0.8–0.9 Å from its position in the native enzyme (Figure 7). The increase of the free energy barrier in the D21E mutant seems to be mainly due to a loss of the Ca^{2+} stabilizing effect at the

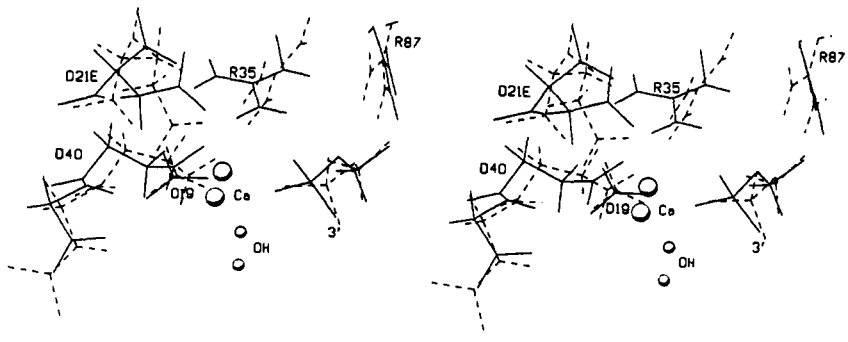

FIGURE 7: Comparison of the native (full lines) and D21E mutant (dashed lines) active site structures after the proton transfer step (state Ψ^g_2). The Ca^{2+} and OH^- ions are represented by solid and dotted circles in the native and mutant enzyme, respectively.

transition state. In addition the OH^- ion appears to be displaced along with the Ca^{2+} ion, which could be interpreted in terms of a less favorable arrangement for the OH^- attack on the phosphate group. This effect, however, is not entropic but rather associated with the dual task of the Ca^{2+} ion in stabilizing both the OH^- ion during the reaction and the extra negative charge on the phosphate group at Ψ_3^g.

Conclusions

We have presented a first attempt to calculate a complete reaction free energy profile for the postulated mechanism of staphylococcal nuclease, using the EVB method in combination with FEP/MD simulations. The results indicate that it is possible to reach quantitative agreement between calculated and observed free energy barriers. It should be emphasized that we are using only the basic reactions in solution as our reference for the enzyme reaction, as compared to simpler calculations where one only considers the effect of mutations using the protein reaction as reference. Thus, the fact that such good agreement with experiment can be obtained is particularly promising.

The calculations give some interesting insights into the details of the postulated mechanism. First, already the general-base catalysis step *in solution* is associated with a free energy barrier that is too high to be consistent with k_{cat} of the enzyme. Therefore, the general-base mechanism itself is not a sufficiently effective way of generating the hydroxide ion for the second step. However, the situation is greatly facilitated by the presence of the Ca^{2+} ion, in particular for stabilizing the OH^- product state of the first step. The fact that the enzyme reaction has an optimum at fairly high pH and that this optimum varies inversely with Ca^{2+} concentration may indicate that the general-base catalysis step is not required at high OH^- concentrations. Also, in view of the extra negative charge of the pdTp inhibitor (compared to a substrate), it is not evident that one can exclude the possibility of a Ca^{2+}-bound OH^- ion in the reactant state (with a true substrate bound to the enzyme), on the basis of the inhibited X-ray structure. It is therefore difficult to discriminate between general-base catalysis mechanism (Cotton et al., 1979) and the initially proposed mechanism (Cotton et al., 1971) with an OH^- bound to the Ca^{2+} in the reactant state. However, our calculations suggest that the reactant and product states of the general-base catalysis step are of similar energy, which would make such a discrimination less crucial.

The importance for an enzyme of being able to provide an electrostatically complementary environment to an ionic transition state structure is well illustrated in the case of SNase. The extreme efficiency with which the positive charges of Arg 35, Arg 87, and the Ca^{2+} ion can stabilize the accumulating double negative charge on the 5′-phosphate group is the major factor responsible for the reduction of the 33 kcal/mol barrier (in solution) by almost 20 kcal/mol. Apparently the protein is capable of providing a polar environment around these charges as well as keeping the effective dielectric constant relatively small for this crucial electrostatic stabilization effect. The FEP/MD simulations show that the hydrogen-bonding interactions between the active site residues and 5′-phosphate are strengthened considerably as the double negative charge is formed. Particularly, Arg 87 donates two hydrogen bonds in the transition state, while it is not interacting as closely in the reactant state. This observation directly supports the revised reaction mechanism for SNase proposed by Sepersu et al. (1987). It is also interesting to note that the Ca^{2+} ion appears to be an important factor along the entire reaction profile. It reduces the energetic cost of the first step to just a few kilocalories, it facilitates the hydrolysis step by approximating and positioning the OH^- ion for the nucleophilic attack, and, more importantly, helps in stabilizing the phosphate charge at the transition state of the second step. Further calculations on the effects of metal ion substitutions should therefore hopefully be able to give quantitative explanations for why this system is so well tailored for Ca^{2+} ions, while not for other divalent cations.

Registry No. L-Arg, 74-79-3; Ca, 7440-70-2; staphylococcal nuclease, 9013-53-0.

References

Albery, J. W., & Kreevoy, M. M. (1978) *Adv. Phys. Org. Chem. 16*, 87–157.

Bunton, C. A., Mhala, M. M., Oldham, K. G., & Vernon, C. A. (1960) *J. Chem. Soc.*, 3293–3301.

Burgess, M. A. (1978) *Metal Ions in Solution*, Ellis Horwood Ltd., Chichester, England.

Chandrasekhar, J., Smith, S. F., & Jorgensen, W. L. (1985) *J. Am. Chem. Soc. 107*, 154–163.

Cotton, F. A., Bier, C. J., Day, V. W., Hazen, E. E., Jr., & Larsen, S. (1971) *Cold Spring Harbor Symp. Quant. Biol. 36*, 243–249.

Cotton, F. A., Hazen, E. E., Jr., & Legg, M. J. (1979) *Proc. Natl. Acad. Sci. U.S.A. 76*, 2551–2555.

Craik, C. S., Largman, C., Fletcher, T., Roczniak, S., Barr, P. J., Fletterick, R., & Rutter, W. J. (1985) *Science 228*, 291–297.

Cronin, C. N., Malcolm, B. A., & Kirsh, J. F. (1987) *J. Am. Chem. 109*, 2222–2223.

Cuatrecasas, P., Fuchs, S., & Anfinsen, C. B. (1967) *J. Biol. Chem. 242*, 1541–1547.

Eigen, M., & de Maeyer, L. (1955) *Z. Elektrochem. 59*, 986–993.

Guthrie, J. P. (1977) *J. Am. Chem. Soc. 99*, 3991–4001.

Hammond, G. S. (1955) *J. Am. Chem. Soc. 77*, 334–338.

Hwang, J.-K., & Warshel, A. (1987a) *J. Am. Chem. Soc. 109*, 715–720.

Hwang, J.-K., & Warshel, A. (1987b) *Biochemistry 26*, 2669–2671.

Hwang, J.-K., King, G., Creighton, S., & Warshel, A. (1988) *J. Am. Chem. Soc. 110*, 5297–5311.

Knowles, J. R. (1987) *Science 236*, 1252–1262.

Kollman, P. A., & Hayes, D. M. (1981) *J. Am. Chem. Soc. 103*, 2955–2961.

Kumamoto, J., Cox, J. R., & Westheimer, F. H. (1955) *J. Am. Chem. Soc. 78*, 4858–4860.

Licheri, G., Piccaluga, G., & Pinna, G. (1976) *J. Chem. Phys. 64*, 2437–2441.

Rao, S. N., Singh, U. C., Bash, P. A., & Kollman, P. A. (1987) *Nature (London) 328*, 551–554.

Sepersu, E. H., Shortle, D., & Mildvan, A. S. (1986) *Biochemistry 25*, 68–77.

Sepersu, E. H., Shortle, D., & Mildvan, A. S. (1987) *Biochemistry 26*, 1289–1300.

Tapia, O., & Johannin, G. (1981) *J. Chem. Phys. 75*, 3624–3635.

Tapia, O., & Lluch, J. M. (1985) *J. Chem. Phys. 83*, 3970–3982.

Tucker, P. W., Hazen, E. E., Jr., & Cotton, F. A. (1978) *Mol. Cell. Biochem. 22*, 67–77.

Tucker, P. W., Hazen, E. E., Jr., & Cotton, F. A. (1979) *Mol. Cell. Biochem. 23*, 67–86.

Valleau, J. P., & Torrie, G. M. (1977) in *Modern Theoretical Chemistry* (Berne, B. J., Ed.) Vol. 5, pp 169–194, Plenum, New York.

van Duijnen, P. Th., Thole, B. Th., & Hol, W. G. J. (1979) *Biophys. Chem. 9*, 273–280.
Warshel, A. (1979) *J. Phys. Chem. 83*, 1640–1652.
Warshel, A. (1981) *Biochemistry 20*, 3167–3177.
Warshel, A. (1982) *J. Phys. Chem. 86*, 2218–2224.
Warshel, A. (1984a) *Proc. Natl. Acad. Sci. U.S.A. 81*, 444–484.
Warshel, A. (1984b) *Pontif. Acad. Sci. Scr. Varia 55*, 59–81.
Warshel, A., & Levitt, M. (1976) *J. Mol. Biol. 103*, 227–249.
Warshel, A., & Weiss, R. M. (1980) *J. Am. Chem. Soc. 102*, 6218–6226.
Warshel, A., & Russell, S. T. (1984) *Q. Rev. Biophys. 17*, 283–422.
Warshel, A., & King, G. (1985) *Chem. Phys. Lett. 121*, 124–129.
Warshel, A., & Russell, S. T. (1986) *J. Am. Chem. Soc. 108*, 6569–6579.
Warshel, A., & Sussman, F. (1986) *Proc. Natl. Acad. Sci. U.S.A. 83*, 3806–3810.
Warshel, A., Russell, S. T., & Sussman, F. (1986) *Isr. J. Chem. 27*, 217–224.
Warshel, A., Sussman, F., & Hwang, J.-K. (1988) *J. Mol. Biol. 201*, 139–159.
Weiner, S. J., Seibel, G. L., & Kollman, P. A. (1986) *Proc. Natl. Acad. Sci. U.S.A. 83*, 649–653.
Wells, J. A., Cunningham, B. C., Graycar, T. P., & Estell, D. A. (1986) *Philos. Trans. R. Soc. London, A 317*, 415–423.
Wilde, J. A., Bolton, P. H., Dell'Acqua, M., Hibler, D. W., Pourmotabbed, T., & Gerlt, J. A. (1988) *Biochemistry 27*, 4127–4132.
Wilkinson, A. J., Fersht, A. R., Blow, D. M., Carter, C., & Winter, G. (1984) *Nature (London) 307*, 187–188.
Zwanzig, R. W. (1954) *J. Chem. Phys. 22*, 1420–1426.

Binding of Thiocyanate to Lactoperoxidase: ^1H and ^{15}N Nuclear Magnetic Resonance Studies

Sandeep Modi, Digambar V. Behere, and Samaresh Mitra*
Chemical Physics Group, Tata Institute of Fundamental Research, Homi Bhabha Road, Colaba, Bombay 400005, India
Received October 5, 1988; Revised Manuscript Received January 12, 1989

ABSTRACT: The binding of thiocyanate to lactoperoxidase (LPO) has been investigated by ^1H and ^{15}N NMR spectroscopy. ^1H NMR of LPO shows that the major broad heme methyl proton resonance at about 61 ppm is shifted upfield by addition of the thiocyanate, indicating binding of the thiocyanate to the enzyme. The pH dependence of line width of ^{15}N resonance of $SC^{15}N^-$ in the presence of the enzyme has revealed that the binding of the thiocyanate to the enzyme is facilitated by protonation of an ionizable group (with pK_a of 6.4), which is presumably distal histidine. Dissociation constants (K_D) of $SC^{15}N^-$/LPO, $SC^{15}N^-$/LPO/I^-, and $SC^{15}N^-$/LPO/CN^- equilibria have been determined by ^{15}N T_1 measurements and found to be 90 ± 5, 173 ± 20, and 83 ± 6 mM, respectively. On the basis of these values of K_D, it is suggested that the iodide ion inhibits the binding of the thiocyanate but cyanide ion does not. The thiocyanate is shown to bind at the same site of LPO as iodide does, but the binding is considerably weaker and is away from the ferric ion. The distance of ^{15}N of the bound thiocyanate ion from the iron is determined to be 7.2 ± 0.2 Å from the ^{15}N T_1 measurements.

Lactoperoxidase (LPO, EC 1.11.1.7, donor:H_2O_2 oxidoreductase) is a heme protein enzyme found in milk, saliva, and tears. In common with other peroxidases, the enzyme catalyzes oxidation of a number of organic and inorganic substrates by hydrogen peroxide and is therefore a component of the biological defense mechanism of mammalians. Of many inorganic substrates, thiocyanate is very attractive because thiocyanate ion/H_2O_2/LPO provides a potent nonspecific bacteriostatic or bacteriocidal system (Reiter et al., 1963, 1976). This system operates in vivo to protect the gut of the calf from enteric pathogens (Reiter et al., 1980; Marshall et al., 1986) and has been used to preserve raw milk without refrigeration (Bjorck et al., 1979). However, the mechanism of the action and oxidation of thiocyanate ion is not yet well understood, although several studies have been reported to elucidate the nature of the active agent(s) in the SCN^-/H_2O_2/LPO system. Chung and Wood (1970) have suggested that the antibacterial action of the system may be due to the cyanide ion produced as one of the oxidation products. Hog and Jago (1970) have, however, proposed from their polarographic studies that cyanosulfurous acid or cyanosulfuric acid may account for its antimicrobial activity. Aune and Thomas (1977) have suggested that $OSCN^-$ may be the relatively stable antimicrobial species that accumulates during peroxidase-catalyzed oxidation of SCN^-. This proposal has been supported by studies of other workers (Hoogendoorn et al., 1977; Marshall & Reiter, 1980). Recently, Magnusson et al. (1984) have studied catalytic activity of LPO using iodide and thiocyanate ions. They have proposed that the oxidation of iodide and thiocyanate with hydrogen peroxide catalyzed by lactoperoxidase and thyroid peroxidase occurs via a two-electron transfer, in contrast to one-electron transfer for more usual aromatic donor molecules, and thus species such as IO^- and $OSCN^-$ may be produced. The mechanism of two-electron transfer is, however, still obscure. To elucidate the mechanism, studies on the interaction of thiocyanate ion and LPO are needed.

In the present study, the interaction of thiocyanate ion with LPO was investigated by use of ^{15}N NMR and ^1H NMR. From the measurements of relaxation times of $(SC^{15}N)^-$ in the presence and absence of LPO, the dissociation constant

* Address correspondence to this author.

0006-2960/89/0428-4689$01.50/0